Quantitative Measurements of Electrocatalytic Reaction Rates with NanoSECM

Gaukhar Askarova,[†,§] *Koushik Barman,*[†] *and Michael V. Mirkin*[†,#,*]

[†] Department of Chemistry and Biochemistry, Queens College, Flushing, NY 11367, USA

[§] The Graduate Center of CUNY, New York, NY 10016

[#] Advanced Science Research Center at The Graduate Center, CUNY; New York, NY 10031

Corresponding Author

E-mail: mmirkin@qc.cuny.edu

FAX: 718-997-5531

ABSTRACT

Scanning electrochemical microscopy (SECM) has been extensively used for mapping electrocatalytic surface reactivity; however, most of those studies were carried out using micrometer-sized tips, and no quantitative kinetic experiments on the nanoscale have yet been reported to date. Because the diffusion-limited current density at a nm-sized electrode is very high, an inner-sphere electron-transfer process occurring at a nanotip typically produces a kinetic current at any attainable overpotential. Here we develop the theory for the substrate generation/tip collection (SG/TC) and feedback modes of SECM with a kinetic tip current and use it to evaluate the rates of hydrogen and oxygen evolution reactions in a neutral aqueous solution from the current-distance curves. The possibility of using chemically modified nanotips for kinetic measurements is also demonstrated. The effect of the substrate size on the shape of the current-distance curves in SG/TC mode SECM experiments is discussed.

Since the introduction of scanning electrochemical microscopy (SECM), surface reactivity imaging has been one of the most promising applications of this technique.[1] The capacity for mapping and quantitatively measuring the rates of heterogeneous electrochemical reactions made SECM a valuable tool for probing electrocatalytic processes and evaluating the activities of various electrocatalysts.[2] Electrochemical mapping of the reaction rates at the active sites of electrocatalysts, including defects, edges, and corners, with nanoscale spatial resolution is crucially important for investigating and improving their activity.[3-5] Numerous recent studies have used SECM to investigate electrocatalytic processes, including oxygen reduction reaction (ORR),[6–9] oxygen evolution reaction (OER),[10-17] hydrogen evolution reaction (HER),[18-28] and hydrogen oxidation reaction (HOR).[23,24,29]

A typical approach to probing a catalytic surface reaction by SECM is to use the tip electrode to oxidize or reduce the reaction product (or/and intermediate) in the substrate generation/tip collection (SG/TC) mode.[2-4] However, reactants, products, and intermediates of various inner-sphere electron transfer (ET) reactions, e.g., oxygen, hydrogen, reactive oxygen species, catechol amines, can passivate the electrode surface.[30] These processes are also sensitive to adsorbed impurities that block active atoms needed to carry out such a reaction.[31] The smaller the tip electrode the stronger the effects of its surface deactivation or contamination, and the harder to measure signals produced by inner-sphere processes. For instance, in the study of HOR at individual nanoparticles using a 90-nm-radius Pt tip by Bard and coworkers,[29] the proton reduction current at the tip exhibited instability and gradual decline. After two-hour-long activation, the tip current became more stable, yet the voltammograms still displayed significant hysteresis. The deactivation of the nanoelectrode surface has also been observed during HER.[32] For water oxidation reaction, the formation of anodic film on the surface caused current instability even at

micron-sized gold tips.[6] While catalytic activity mapping with nanotips has been reported,[14,25,26,28,33] these images have likely been affected by tip current instability, making quantitative kinetic measurements in such systems problematic.

To overcome these problems, we recently introduced carbon and Pt nanoelectrodes chemically modified with different surface-bound redox molecules, which enable mediated ET between the electrode surface and dissolved electroactive species.[32] For instance, nanoelectrodes modified with ferrocene (Fc) can oxidize hydrogen[32] or hydrogen peroxide[34] and be used as nanotips for probing HER or ORR. One hurdle in using chemically modified tip is that the rate of mediated ET is typically too slow to attain the diffusion limiting current because the steady-state diffusion current density at a nm-sized electrode is very high (the same is true for inner-sphere ET processes, such as ORR, which produce a kinetic current at a nanotip at any feasible overpotential). The currently available SECM theory is based on the assumption that either the substrate or the tip process is diffusion limited,[35] and no treatment is available for SG/TC mode experiments with kinetically controlled tip and substrate currents.

The focus of this Article is on probing OER and HER occurring during the overall water splitting in a neutral aqueous solution containing no added redox mediator – a practically important system employed for photochemical fuel generation.[36] We develop the theory for three types of SECM experiments with kinetic tip current (Figure 1). In the feedback mode experiment (Figure 1A), O_2 dissolved in solution is reduced at the tip, and the tip potential (E_T) is such that the tip current (i_T) is only due to kinetically controlled ORR at its surface. When the separation distance between the tip and substrate (d) is small (i.e., comparable to tip radius, a), i_T decreases with decreasing d because of the hindered diffusion of O_2 (negative feedback; the tip current near the

surface is lower than in the bulk solution; $i_T < i_{T,\infty}$), since no oxygen regeneration occurs on the substrate.

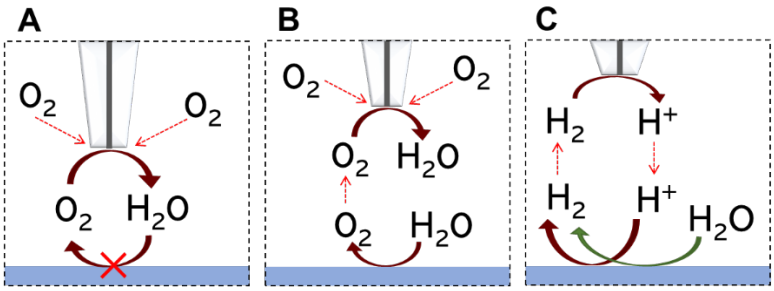

Figure 1. Schematic representation of SECM experiments used for studying water splitting processes in a neutral aqueous solution. (A) Negative SECM feedback based on ORR at the tip. (B) SG/TC of O_2 coupled with the diffusion of dissolved oxygen to the tip. (C) SG/TC of H_2 coupled with the positive SECM feedback due to the H_2 oxidation at the tip and proton reduction at the substrate surface. Not to scale.

In the substrate generation/tip collection (SG/TC) mode of SECM, the tip collects a product of water oxidation or reduction that occurs on the substrate surface. At a negative E_T, oxygen is reduced at the tip surface (Figure 1B), while at a positive E_T, the tip collects H_2 produced by the substrate (Figure 1C). The HOR occurring at the tip produces protons that diffuse to the substrate surface and get reduced back to H_2. This process results in the positive SECM feedback coupled with the SG/TC process, as shown in Figure 1C. The tip current can be recorded either as a function of d (approach curve) or tip x–y position (imaging).

THEORY

The existing SECM theory is mostly applicable to feedback-mode experiments employing outer-sphere redox mediators, and either the tip or the substrate reaction has typically been treated as a diffusion-controlled process.[35] We carried out COMSOL simulations to develop a theory for finite irreversible tip kinetics and an insulating substrate (Figure 1A) and two kinds of SG/TC experiments (Figs. 1B and 1C).

Negative feedback mode of SECM with finite ORR kinetics on the tip. Pure negative feedback is typically used to establish the zero tip–substrate separation point and image the sample topography. In studies of electrocatalytic and photochemical reactions, the addition of a reversible redox mediator to the solution can affect the process kinetics, and a better choice is to use dissolved oxygen for tip positioning and distance measurements. Although the electrocatalytic mechanism of ORR occurring at the tip surface is complicated and not completely known, the kinetic current density can be defined as:

$$j(r,d) = nFk_{T}c_{O_2}(r,d) \quad (1)$$

where r and z are the co-ordinates in the directions radial and normal to the tip surface, respectively, $z = d$ corresponds to the tip surface and $z = 0$ – to of the substrate surface; n is the number of transferred electrons (i.e., 4 for ORR at a Pt tip), F is the Faraday constant, k_T is the effective heterogeneous rate constant at a specific E_T value, and $c_{O_2}(r,d)$ is the local O_2 concentration at the tip. The k_T value determines the ratio of the kinetic tip current to the diffusion-limited ORR current at the same tip ($i_{T,\infty}/i_{T,d}$) in the bulk solution, where

$$i_{T,\infty} = 2\pi \int_0^a \mathrm{r} j(r) d\mathrm{r} \quad (2)$$

$$i_{T,d} = 4xnFaD_{O_2}c^{\circ} \quad (3)$$

x is a function of RG (= r_g/a, i.e., the ratio of glass radius to that of the conductive disk of the tip),[37] $D_{O_2} = 2.4 \times 10^{-5}$ cm^2/s [38] and c° are the diffusion coefficient and bulk concentration of O_2 in solution, respectively. $c^{\circ} = 0.25$ mM was calculated for a 0.1 M K_2SO_4 aqueous solution using the concentration of oxygen in air-saturated pure water (0.27 mM[39,40]) at room temperature and the reported dependence of O_2 solubility on K_2SO_4 concentration.[41]

Three families of dimensionless approach curves ($i_T/i_{T,\infty}$ *vs.* d/a) were calculated for different values of $i_{T,\infty}/i_{T,d}$ ratio and RG (Figure 2). The formulation of the diffusion problem for

the negative feedback mode of SECM with ORR is given in the Supporting Information. For a given RG, there is a unique correspondence between the $i_T/i_{T,\infty}$ value and the dimensionless rate constant ($K_T = k_T a/D_{O_2}$) of ORR (Table S1). While K_T is a general parameter defining the ORR kinetics at the tip, $i_{T,\infty}/i_{T,d}$ values are readily accessible by dividing the experimental $i_{T,d}$ measured in the bulk solution by the $i_{T,d}$ value calculated from Eq. (3) for a given tip. Clearly, the shape of the approach curves in Figure 2 depends strongly on both the ORR kinetics and the RG value. The higher the K_T value (and the corresponding $i_{T,\infty}/i_{T,d}$ ratio), the more significant the mass-transfer limitations at the tip, and the stronger the effect hindered diffusion on the tip current. A larger RG value also results in stronger diffusion blocking and, thus, lower normalized tip current at a given d/a. Taking these factors into account is essential for avoiding significant errors in evaluated d values, which led some authors to conclude that using ORR-based approach curves for distance determination is not reliable.[42]

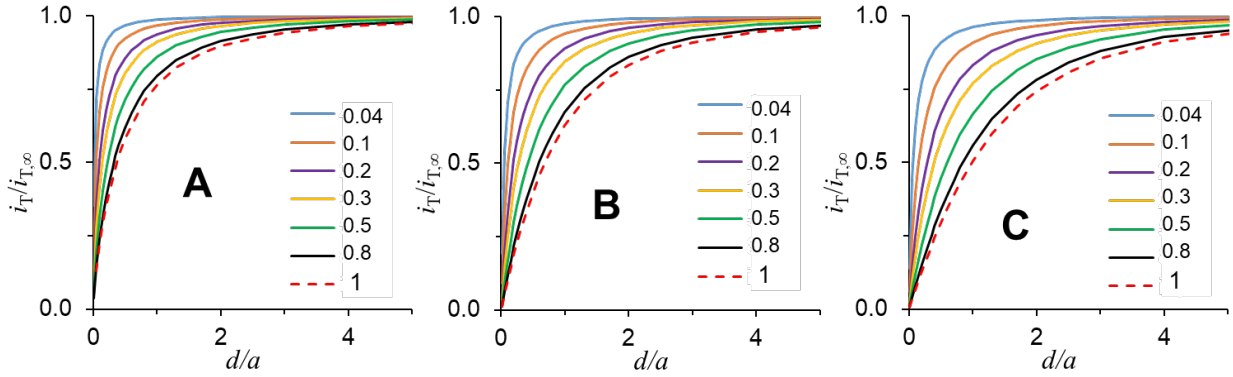

Figure 2. Simulated dimensionless current *vs.* distance curves for a disk-shaped tip with RG = 1.5 (A), 4 (B), and 10 (C) approaching an inert substrate in solution containing oxygen. From top to bottom, $i_{T,\infty}/i_{T,d}$ = 0.04, 0.1, 0.2, 0.3, 0.5, 0.8, and 1 (dashed curve; diffusion-limited tip current).

SG/TC mode of SECM with OER at the substate. Unlike negative SECM feedback considered above, the shape of SG/TC approach curves depends on the substrate size. Because of space limitations, we will consider in more detail the theoretical results for a micron-sized substrate

(substrate radius, a_S = 2 μm), which are relevant to our recent studies of the complete water splitting on semiconductor microcrystals[43,44] and also used for fitting the experimental data reported below. Two other cases, i.e., SG/TC experiments at macroscopic (a_S = 1 mm) and nanoscopic (a_S = 100 nm) substrates, are presented in Supporting Information.

Because the oxidation of water molecules involves no diffusion limitations, we assume that the O_2 flux is uniform over the entire substrate surface. The changes in i_T with d, in this case reflect the competition between two opposing effects: generation of oxygen at the substrate and hindered diffusion of dissolved O_2 from the bulk solution to the tip surface (Figure 1B). The former produces a slow increase in i_T with decreasing d at longer separation distances, while the latter results in a lower i_T at shorter d, where the diffusion blocking by the substrate is most significant.

For a given substrate size, the shape of the approach curves is largely determined by two parameters, i.e., the flux of O_2 generated at the substrate (f_{O_2}) and the K_T (or the corresponding $i_{T,\infty}/i_{T,d}$) value, and the interplay between these factors complicates the analysis. If the tip process is diffusion-limited ($i_{T,\infty}/i_{T,d}$ =1; Figure 3A), the dimensionless current-distance curves simulated for different f_{O_2}values pass through a maximum whose height increases with the oxygen flux at the substrate. The larger the f_{O_2} value, the more significant the contribution of the generated oxygen to the tip current, and the higher the normalized tip current value at a given d/a. The position of the current maximum depends on the substrate radius (a_S = 2 μm in Figure 3).

With moderately fast tip kinetics ($i_{T,\infty}/i_{T,d}$ =0.3; Figure 3B), the shape of the approach curves is qualitatively similar to that in Figure 3A, but the diffusion layer at the tip is thinner, and blocking of oxygen diffusion from the bulk solution by the substrate is significant only at short d. Hence, the current maxima in Figure 3B occur at much shorter separation distances than in Figure

3A. At a much slower tip kinetics ($i_{T,\infty}/i_{T,d}$ = 0.04; Figure 3C), the blocking effect is so weak that the current increases monotonically with decreasing d, and the current maximum can be observed only at a very small f_{O_2} value (e.g., 1.7 nmol cm^{-2} s^{-1}; yellow curve).

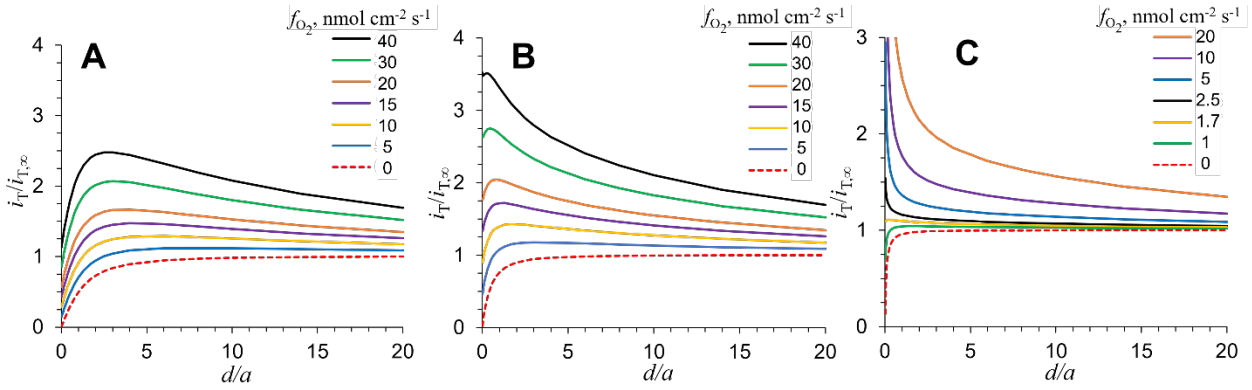

Figure 3. Simulated dimensionless current *vs.* distance curves for ORR at a disk-shaped tip approaching the substrate oxidizing water in solution containing 0.25 mM O_2. $i_{T,\infty}/i_{T,d}$ = 1 (A), 0.3 (B; K_T=0.5550), and 0.04 (C; K_T=0.0524). From top to bottom, the flux of O_2 generated at the substrate, f_{O_2}, nmol cm^{-2} s^{-1} = 40, 30, 20, 15, 10, 5, and 0 (dashed curve – negative feedback). The two top curves are not shown in C. a = 100 nm, RG = 10.

The effect of tip kinetics is clearer in a family of SG/TC mode approach curves simulated for a constant f_{O_2}, and different K_T values (Figure 4). With a moderate flux (f_{O_2} = 5 nmol cm^{-2} s^{-1}) and rapid ORR kinetics at the tip ($i_{T,\infty}/i_{T,d}$ = 1; dashed curve), the tip current decreases monotonically with decreasing d at relatively short d/a, and the shape of the approach curve is similar to that for pure negative feedback. At slower tip kinetics, the diffusion blocking effect is less pronounced, and the approach curve exhibits a maximum (green curve), or even a monotonic increase in i_T with decreasing d (yellow curve). However, even at a very small d, the tip current remains much lower that the diffusion-limited oxygen current in the bulk solution (e.g., $i_T/i_{T,\infty}$= 2 in the yellow curve corresponds to i_T = 0.08$i_{T,d}$).

Thorough characterization of the tip, including independent evaluation of a and RG, is critical for quantitative measurements of OER because these parameters cannot be accurately

determined from kinetic tip current. The dependence of the shape of the approach curves on RG is complicated (Figure S1) because of different effects of this parameter on the collection of the O_2 flux by the tip and the diffusion blocking.

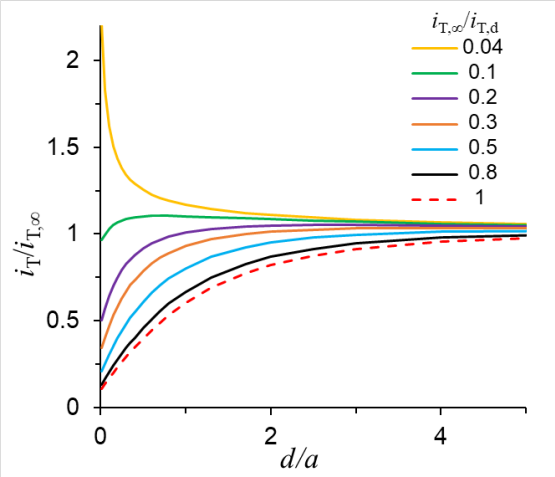

Figure 4. The effect of ORR kinetics at the SECM tip on the shape of approach curves. The dimensionless current-distance curves were simulated for ORR at a disk-shaped tip approaching the substrate oxidizing water in solution containing 0.25 mM O_2. f_{O_2} = 5 nmol cm^{-2} s^{-1}, a = 100 nm, RG = 10. From top to bottom, $i_{T,\infty}/i_{T,d}$ = 0.04, 0.1, 0.2, 0.3, 0.5, 0.8 and 1 (dashed curve; diffusion-limited tip current); the corresponding k_T values are: 0.17, 0.46, 1.05, 1.8, 4.4, 20, and 1000 cm/s.

The SECM theory has previously been developed for feedback mode experiments at either a biased[45] or an unbiased[46] finite disk-shaped substrate. For OER under SG/TC conditions, the size of the conductive portion of the substrate affects the shape of approach curves in two ways – through the magnitude of the O_2 concentration near its surface and the thickness of the substrate-generated diffusion layer. With a 100-nm-radius substrate (i.e., the substrate radius equal to a; Figure S2A), the diffusion layer of generated O_2 is very thin and its concentration near the substrate surface is only slightly higher than the bulk value. Thus, the diffusion blocking dominates even at the O_2 flux values as high as 100 nmol cm^{-2} s^{-1}, and a significant increase in the tip current is

expected only at very short d and extremely high f_{O2} (e.g., 500 nmol cm^{-2} s^{-1}), as compared to the approach curves at a μm-sized substrate (Figure S2B), where the diffusion layer is much thicker, and a much smaller flux of oxygen is needed for i_T to increase near the sample surface. Finally, in Figure S2C the tip travels through a very thick diffusion layer of oxygen generated at a macroscopic substrate. The O_2 concentration does not change much on the micron scale, and i_T is almost constant until the onset of the diffusion blocking at *d/a ca.* 2 to 4. One should notice that the O_2 concentrations in the vicinity of the substrate are very high even at modest flux values (e.g., c_{O2} is ~25 times the bulk value at f_{O2} = 2 nmol cm^{-2} s^{-1}; orange curve in Figure S2C), which may cause bubble formation at relatively low anodic overpotentials.

Steady-state i_T-d curves for SG/TC mode and feedback due to HER at the substate. The current-distance curves simulated for the HER process at the substrate in a neutral aqueous solution (Figure 5) are strikingly different from those computed for OER due to the unusual combination of the SG/TC mode and positive SECM feedback (Figure 1C). When the tip is biased at a positive potential for HOR, $i_{T,\infty}$ is close to zero because there is essentially no hydrogen in the bulk solution. With the tip far from the substrate, the reduction of water molecules, which is not limited by diffusion, produces a uniform H_2 flux over the entire substrate surface. At relatively short d (i.e., less than or comparable to a), i_T increases sharply due to the onset of positive feedback caused by enhanced hydrogen regeneration at the substrate via the oxidation of protons produced at the tip (Figure 1C). The strong dependence of the tip current on the flux of hydrogen generated by water reduction at the substrate (f_{H2}; Figure 5A) enables the evaluation of the HER rate by fitting an experimental current-distance curve to the theory. A higher flux of H_2 causes the tip current to increase at longer separation distances. Thus, the smaller the f_{H2} value the shorter the separation distance at which the HOR current at the tip becomes measurable (e.g., ~1 pA) and the steeper the

approach curve near the substrate surface. For instance, with a flux of 30 nmol cm^{-2} s^{-1} (blue line, Figure 5A), i_T = 1 pA can be measured at d > 400 nm, whereas at a lower flux of 1 nmol cm^{-2} s^{-1} (green line in Figure 5A), the same tip current value corresponds to $d \approx 3$ nm. This behavior was observed experimentally in our SECM studies of water splitting at semiconductor microcrystals,[43,44] where relatively small hydrogen fluxes (ca. 1 nmol cm^{-2} s^{-1}) could be measured only at very short separation distances.

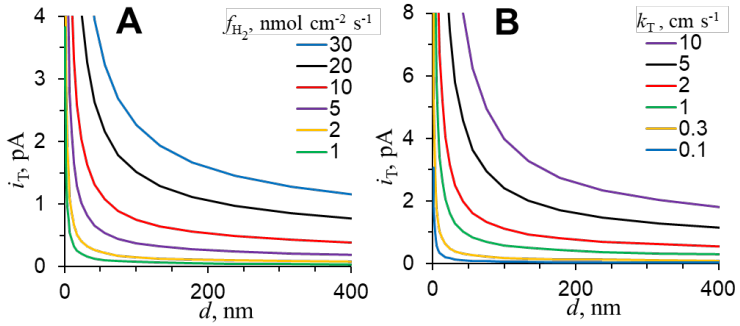

Figure 5. Simulated current *vs.* distance curves for HOR at a disk-shaped tip approaching the substrate that generates hydrogen. (A) From top to bottom, the flux of H_2 generated at the substrate, f_{H_2}, nmol cm^{-2} s^{-1} = 30, 20, 10, 5, 2, and 1; k_T = 0.25 cm/s. (B) From top to bottom, k_T, cm/s = 10, 5, 2, 1, 0.3, and 0.1; f_{H_2} = 2 nmol cm^{-2} s^{-1}. a = 100 nm, RG = 10. The substrate radius, a_S = 2 μm. The ranges of k_T and f_{H_2} in panels A and B, respectively, cover the values used for fitting experimental current-distance curves (see below).

The HOR current at the tip is kinetic and depends on the effective rate constant (k_T; Figure 5B). As expected, the faster the HOR kinetics at the tip, the more efficiently the tip collects H_2, and the longer the separation distance at which the hydrogen flux generated at the substrate can be measured. When the HOR rate is lower, a tip can only detect hydrogen in very close proximity to the substrate, which is technically challenging. Fabricating nanotips exhibiting sufficiently fast HOR kinetics is not straightforward because k_T is directly proportional to the tip surface coverage of a redox mediator, which is not easy to increase.

The substrate size greatly affects the shape of the current-distance curves, and the interplay between this parameter and the k_T and f_{H_2} values is illustrated in Figure S3. The approach curves simulated for a tip collecting hydrogen generated at a nanoscopic (a_S = 100 nm; Figure S3, panels A, D, and G), a microscopic (a_S = 2 μm; Figure S3, panels B, E, and H), and a macroscopic (a_S = 1 mm; Figure S3, panels C, F, and I) substrate reflect the differences in the diffusion layer thickness and the H_2 concentration profile. The smaller the substrate radius, the thinner the diffusion layer of H_2, and steeper the gradient of its concentration at the substrate surface. Clearly, it is easier to measure the hydrogen flux at a mm-sized substrate, where the concentration of H_2 changes very slowly with d within a thick diffusion layer (Figs. S3C, S3F, and S3I). The high concentration of hydrogen near a large substrate results in a high tip current even for small f_{H_2} values. When k_T is small (Figs. S3C) i_T is essentially independent of d until the tip comes very close to the substrate, and f_{H_2} can be determined from the well-defined i_T value. The larger the k_T value the more significant positive feedback due to the formation of protons at the tip and their reduction at the substrate surface (cf. Figs. S3F and S3I).

With the nanoscopic substrate (Figs. S3A, S3D, and S3G), the concentration of hydrogen generated near its surface is relatively low, the diffusion layer is thin, and the tip current is measurable only within the range d equivalent to a few tip radii. The approach curves are steep, and the entire curve must be fitted theory to evaluate the generated hydrogen flux. If f_{H_2} is not very large (e.g., <100 nmol cm^{-2} s^{-1}) and/or the HOR kinetics at the tip is not very fast (Figs. S3A and S3D), the tip has to be brought within a few nm distance from the substrate, where i_T is amplified by positive feedback. The responses simulated for a micrometer-size substrate (Figs. S3B, S3E, and S3H) are intermediate between the two extreme cases discussed above. The effect

of RG on the approach curves in the SG/TC mode is relatively small for HER and may not be apparent in experiments.

EXPERIMENTAL SECTION

Chemicals. Potassium sulfate (99%), (6-bromohexyl)ferrocene, tetrabutylammonium tetrafluoroborate ($TBABF_4$, 99%), boric acid (≥99.5%), sodium hydroxide, sodium sulfate (≥ 99.0%), and acetonitrile (≥99.9%), all from Sigma Aldrich, were used as received. Ferrocenemethanol (FcMeOH; 97%, Alfa Aesar) was sublimed before the experiments. A phosphate buffer (pH 7) solution was prepared from sodium phosphate monobasic monohydrate (98%, FisherBiotech) and sodium phosphate dibasic heptahydrate (99%, FisherBiotech). Aqueous solutions for SECM experiments were prepared using deionized water from the Milli-Q Advantage A10 system equipped with Q-Gard T2 Pak, a Quantum TEX cartridge, and a VOC pak; total organic carbon (TOC) <3 ppb.

Fabrication of Pt nanoelectrodes. Disk-type Pt nanoelectrodes were fabricated by pulling 25-μm-diameter annealed Pt wires (Goodfellow) into borosilicate capillaries (Drummond; O D, 1.0 mm; ID, 0.2 mm) with the help of a P-2000 laser puller (Sutter Instrument Co.).[47] The pulled tips were polished on a 50 nm alumina disk (Precision Surfaces International) under video microscopic control and sonicated in deionized water for 10 s. A microforge (model MF-900, Narishige, Tokyo, Japan) was used to reduce the RG (i.e., the ratio of glass radius to that of the conductive tip) of the tapered tip. The appropriate protection was used to avoid electrostatic damage to the nanoelectrodes.[48] The tip size and shape were evaluated from TEM images and SECM approach curves.[49]

Modification of Pt nanoelectrodes. Ferrocene was attached to a Pt nanoelectrode surface using an earlier reported procedure for the reduction of primary monohaloalkanes.[50] A Pt

nanoelectrode was biased at a negative potential (-2.0 V *vs.* $Ag/AgNO_3$) for 20 seconds in acetonitrile solution of 5 mM (6-bromohexyl)ferrocene containing 0.1 M $TBABF_4$ under an inert atmosphere. The modified electrodes were washed carefully with acetonitrile and water. While ORR occurred at the Pt surface, and its current was not greatly affected by chemical modification, HOR was mediated by the surface-bound Fc molecules.[32] A current vs. time curve illustrating the response stability of a Fc-modified SECM nanotip is shown in Figure S7.

SECM setup and procedures. SECM experiments were carried out using a previously described home-built instrument.[51] The 4-electrode arrangement was employed with either a commercial mercury/mercurous sulfate reference electrode (CH Instruments, model CHI 151) or a silver/silver chloride reference electrode (CH Instruments, model CHI 111), and a Pt wire serving as a counter electrode. A 5-μm-radius Pt ultramicroelectrode (UME; CH Instruments, model CHI 107) was polished before the experiment. The nanoelectrode tip was initially positioned a few tens of micrometers above Pt UME substrate with the help of a long-distance video microscope. A digital angle gauge (DWL-80Pro, Digi-Pas) was used to ensure the horizontal orientation of the substrate plane and the correct tip/substrate alignment. A current *vs.* distance curve was obtained during the subsequent fine approach. All experiments were carried out in a Faraday cage at room temperature (23 ± 2 ºC). The current offset of the potentiostat (~2 pA) was subtracted from all measured current values.

In the negative feedback mode, a nanotip was biased at -0.95 V *vs*. Hg/Hg_2SO_4 for ORR to occur on its surface. Using the SG/TC mode for OER studies, the Pt UME substrate was biased at 0.8 V *vs*. Hg/Hg_2SO_4 for water oxidation, and the tip was biased at -0.95 Hg/Hg_2SO_4 to collect the generated oxygen. Using the SG/TC mode for HER studies, the substrate was biased at -1.4 V *vs*. Hg/Hg_2SO_4 for water reduction, and the tip was biased at 0.4 V *vs*. Hg/Hg_2SO_4 to collect the

generated hydrogen. No oxygen or hydrogen bubble formation was detected in SECM experiments at the selected potentials and under given conditions.

Finite-element simulations. Simulations were carried out using COMSOL Multiphysics commercial package, version 6.1. Axisymmetric 2D models were built to simulate the SECM experiments, including negative feedback and SG/TC modes. The "transport of dilute species" model was used to solve steady-state diffusion problems. The COMSOL modeling reports are available in the Supporting Information.

RESULTS AND DISCUSSION

To demonstrate the feasibility of quantitative SECM experiments with a kinetically controlled tip process, we fitted an experimental approach curve based on ORR at the tip (a = 74 nm, RG = 4) to the negative feedback theory developed above (Figure 6A). The kinetic tip current far away from the substrate ($i_{T,\infty}$ = 18.5 pA) was significantly lower than the value of the diffusion-limited current of dissolved O_2 ($i_{T,d}$ =71.8 pA) calculated from Eq. (3), corresponding to $i_{T,\infty}/i_{T,d}$ = 0.26. To validate these parameters, an approach curve based on the diffusion-limited current of ferrocene methanol (FcMeOH) oxidation at the same tip approaching the same glass substrate was

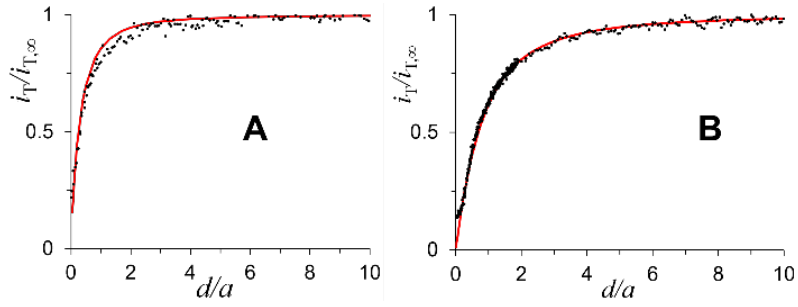

Figure 6. Experimental (symbols) and theoretical (solid lines) i_T–d curves obtained with the same microforged Pt tip approaching a glass surface. Both theoretical curves were calculated for a = 74 nm and RG = 4. (A) The tip current is due to ORR in 0.1 M PB solution (pH 7). E_T = -0.8 V *vs.* Ag/AgCl. $i_{T,\infty}/i_{T,d}$ = 0.26. (B) i_T is due to the oxidation of 1 mM FcMeOH in 0.1 M PB solution. $i_{T,\infty} = i_{T,d}$. E_T = 0.4 V.

fitted to the conventional SECM theory[52] using the same a and RG values (Figure 6B). Clearly, ORR-based approach curves obtained in the negative feedback mode can be used for establishing the d scale and precisely evaluating the tip/substrate separation distance, which is required for the accurate quantitative analysis of substrate kinetics. An additional example of fitting an experimental ORR-based approach curve to the theory with a significantly larger tip radius value (a = 160 nm) validated by TEM is shown in Figure S4.

Figure 7 shows a current-distance curve obtained with a Fc-modified Pt tip approaching a micron-sized Pt substrate electrode biased at E_s = 0.8 V *vs.* Hg/Hg_2SO_4 to generate oxygen in 0.1 M borate buffer solution (pH 8.5) containing 0.5 M Na_2SO_4. The fit of the experimental approach curve (black symbols) to the simulated one (red solid line) yielded f_{O_2} = 0.6 nmol cm^{-2} s^{-1}. This small flux is due to the low E_s value selected to prevent the formation of oxygen bubbles. Measuring such a small flux was especially difficult because of the slow ORR kinetics at the tip (*cf.* $i_{T,\infty}/i_{T,d}$ = 0.05 in Figure 7 and $i_{T,\infty}/i_{T,d}$ = 0.26 in Figure 6A).

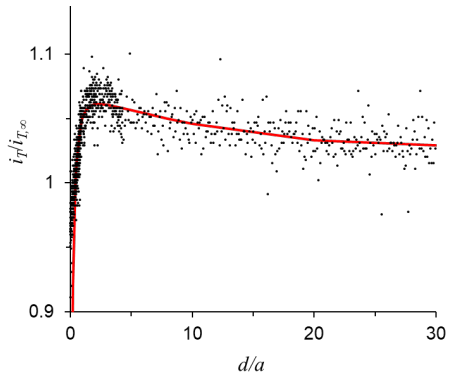

Figure 7. Experimental i_T–d curve (symbols) obtained with a Fc-modified Pt tip approaching a Pt UME substrate and fitted to the theory (solid line). Theoretical curve was calculated for a = 305 nm and RG = 5. The 0.1 M borate buffer solution (pH 8.5) in 0.5 M Na_2SO_4 contained no redox species other than dissolved O_2. E_T = -0.95 V, E_s = 0.8 V *vs.* Hg/Hg_2SO_4. $i_{T,\infty}/i_{T,d}$ = 0.05 (k_T = 0.055 cm/s), f_{O_2} = 0.6 nmol cm^{-2} s^{-1}. The approach velocity was decreased from 50 nm/s to 10 nm/s at $d/a \approx 4$.

The developed theory is applicable to a disk-shaped tip made from any suitable metal or carbon, either bare or chemically modified. The k_T value for ORR at the tip needs to be determined independently prior to fitting an approach curve. An approach curve obtained with a Fc-modified carbon nanotip (symbols) and fitted to the theory (solid line) is shown in Figure S5.

HOR at a ferrocene-modified nanotip occurs via a mediated electron-transfer process, and the k_T value is largely determined by the density of the attached Fc molecules and varies significantly for different tips. Prior to measuring HER kinetics, the zero-separation point was determined and the distance scale established using ORR-based approach curves in the negative feedback mode (data not shown). The two experimental SG/TC mode approach curves (Figure 8)) were obtained at E_T = 0.4 V *vs.* Hg/Hg_2SO_4 and E_S = -1.3 V *vs.* Hg/Hg_2SO_4 (Figure 8A) and -1.4 V (Figure 8B) and fitted to the theory (solid red lines) to determine the flux of hydrogen generated by the reduction of water at the substrate, f_{H_2} = 9 nmol cm^{-2} s^{-1} and 17 nmol cm^{-2} s^{-1}, respectively.

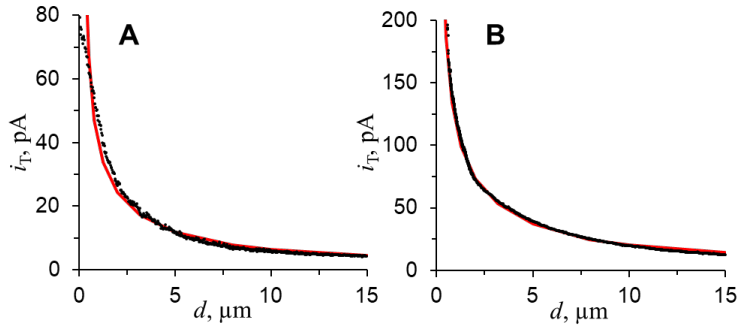

Figure 8. Experimental (symbols) and theoretical (solid lines) i_T–d curves obtained with Fc-modified Pt tip approaching a Pt UME substrate. Both theoretical curves were calculated for a = 400 nm and RG = 10. (A) k_T = 0.5 cm/s, f_{H_2} = 9 nmol cm^{-2} s^{-1}, E_T = 0.4 V, E_S = -1.3 V *vs.* Hg/Hg_2SO_4. (B) k_T = 1 cm/s, f_{H_2} = 17 nmol cm^{-2} s^{-1}, E_T = 0.4 V, E_S = -1.4 V *vs.* Hg/Hg_2SO_4. The tip current is due to HOR in 0.1 M PB solution (pH 7).

The f_{H_2} value extracted from the fit can be validated by comparing it to hydrogen flux determined independently from the substrate current. In Figure S6, the ORR current density measured on the substrate (5.86 mA cm^{-2}) was subtracted from the total substrate current density of 6.75 mA cm^{-2}. The resulting value (0.89 mA cm^{-2}) corresponds to f_{H2} = 4.62 nmol cm^{-2} s^{-1}. This f_{H2} value was used to simulate the theoretical curve (red line in Figure S6) in good agreement with the experimental approach curve (symbols).

CONCLUSIONS

To realize the SECM potential for mapping active sites on electrode surfaces and quantitatively evaluating electro(photo)catalytic activity with a nanoscale resolution, one has to measure fluxes of products and/or reactants and intermediates of such processes with nanometer-sized tip electrodes. Measuring inner-sphere charge-transfer reactions at nanotips presents significant technical challenges, including rapid passivation or contamination of the nanoelectrode surface that necessitates the use of chemically modified nanoprobes. Electrocatalytic processes at either bare or chemically modified nanotips typically produce kinetic rather than diffusion-limited currents. We carried out finite-element simulations to develop the theory for water splitting on the substrate surface probed in a SG/TC mode coupled with either negative (oxygen detection) or positive (hydrogen detection) SECM feedback and kinetic tip current. Although the water splitting processes are not diffusion controlled, and the generated O_2 and H_2 fluxes are uniform over the substrate surface, the concentration profiles in solution and the shape of the SECM current-distance curves depend strongly on the substrate size. Experimental curves obtained for HER and OER were fitted to the theory to measure the rates of these processes at a micron-sized substrate.

■ ASSOCIATED CONTENT

Supporting Information. Formulation of the diffusion problem, Table S1, Figures S1 – S3, and

COMSOL simulation reports. This material is available free of charge via the Internet at http://pubs.acs.org.

AUTHOR INFORMATION

Corresponding Author

*E-mail: mmirkin@qc.cuny.edu. Fax: 718-997-5531.

Author Contributions

All authors have given approval to the final version of the manuscript.

Notes

The authors declare no competing financial interest.

ACKNOWLEDGMENTS

The support of this work by the National Science Foundation grant CHE-2102298 is gratefully acknowledged.

REFERENCES

1. Bard, A. J.; Fan, F.-R. F.; Pierce, D. T.; Unwin, P. R.; Wipf, D. O.; Zhou, F. Chemical Imaging of Surfaces with the Scanning Electrochemical Microscope. *Science* **1991**, *254*, 68.
2. Ahn, H. S.; Zoski, C. G.; Bard, A. J. Electrocatalysis and Surface Interrogation. In Scanning Electrochemical Microscopy, 3rd ed.; Bard, A. J.; Mirkin, M. V., Eds.; CRC Press: Boca Raton, 2022, pp. 127–153.
3. Bentley, C. L.; Edmondson, J.; Meloni, G. N.; Perry, D.; Shkirskiy, V.; Unwin, P. R. Nanoscale Electrochemical Mapping. *Anal. Chem.* **2019,** *91*, 84–108.
4. Wang, X.; Askarova, G.; Mirkin, M. V. Electrochemical Microscopy at the Nanoscale. In Nanoscale Electrochemistry; Wain, A.; Dickinson, E. Eds., Elsevier Ltd., 2021, pp. 129–202.
5. Santana Santos, C.; Jaato, B. N.; Sanjuán, I.; Schuhmann, W.; Andronescu, C. Operando Scanning Electrochemical Probe Microscopy during Electrocatalysis. *Chem. Rev.* **2023**, *123*, 4972–5019.
6. Liu, B.; Bard, A. J. Scanning Electrochemical Microscopy. 45. Study of the Kinetics of Oxygen Reduction on Platinum with Potential Programming of the Tip. *J. Phys. Chem. B* **2002**, *106*, 12801–12806.

7. Fernández, J. L.; Bard, A. J. Scanning Electrochemical Microscopy. 47. Imaging Electrocatalytic Activity for Oxygen Reduction in an Acidic Medium by the Tip Generation−Substrate Collection Mode. *Anal Chem* **2003**, *75*, 2967–2974.

8. Sánchez-Sánchez, C. M.; Rodríguez-López, J.; Bard, A. J. Scanning Electrochemical Microscopy. 60. Quantitative Calibration of the SECM Substrate Generation/Tip Collection Mode and its Use for the Study of the Oxygen Reduction Mechanism. *Anal. Chem.* **2008**, *80*, 3254–3260.

9. Eckhard, K.; Chen, X.; Turcu, F.; Schuhmann, W. Redox Competition Mode of Scanning Electrochemical Microscopy (RC-SECM) for Visualisation of Local Catalytic Activity. *Phys. Chem. Chem. Phys.* **2006**, *8*, 5359–5365.

10. Fushimi, K.; Okawa, T.; Seo, M. A Scanning Electrochemical Microscopic Observation of Heterogeneous Oxygen Evolution on a Polycrystalline Titanium during Anodic Oxidation. *Electrochemistry* **2000**, *68*, 950–954.

11. Minguzzi, A.; Alpuche-Aviles, M. A.; López, J. R.; Rondinini, S.; Bard, A. J. Screening of Oxygen Evolution Electrocatalysts by Scanning Electrochemical Microscopy Using a Shielded Tip Approach. *Anal. Chem.* **2008**, *80*, 4055–4064.

12. Minguzzi, A.; Battistel, D.; Rodríguez-López, J.; Vertova, A.; Rondinini, S.; Bard, A. J.; Daniele, S. Rapid Characterization of Oxygen-Evolving Electrocatalyst Spot Arrays by the Substrate Generation/Tip Collection Mode of Scanning Electrochemical Microscopy with Decreased O_2 Diffusion Layer Overlap. *J. Phys. Chem. C* **2015**, *119*, 2941–2947.

13. Counihan, M. J.; Setwipatanachai, W.; Rodríguez-López, J. Interrogating the Surface Intermediates and Water Oxidation Products of Boron-Doped Diamond Electrodes with Scanning Electrochemical Microscopy. *ChemElectroChem* **2019**, *6*, 3507–3515.

14. Sun, T.; Wang, D.; Mirkin, M. V.; Cheng, H.; Zheng, J.-C.; Richards, R. M.; Lin, F.; Xin, H. L. Direct High-Resolution Mapping of Electrocatalytic Activity of Semi-Two-Dimensional Catalysts with Single-Edge Sensitivity. *Proc. Natl. Acad. Sci. USA* **2019**, *116*, 11618–11623.

15. Ju, M.; Cai, R.; Ren, J.; Chen, J.; Qi, L.; Long, X.; Yang, S. Conductive Polymer Intercalation Tunes Charge Transfer and Sorption–Desorption Properties of LDH Enabling Efficient Alkaline Water Oxidation. *ACS Appl. Mater. Interfaces* **2021**, *13*, 37063–37070.

16. Bae, J. H.; Nepomnyashchii, A. B.; Wang, X.; Potapenko, D. V.; Mirkin, M. V. Photo-Scanning Electrochemical Microscopy on the Nanoscale with Through-Tip Illumination. *Anal. Chem.* **2019**, *91*, 12601–12605.

17. Sarkar, S.; Wang, X.; Hesari, M.; Chen, P.; Mirkin, M. V. Scanning Electrochemical and Photoelectrochemical Microscopy on Finder Grids: Toward Correlative Multitechnique Imaging of Surfaces. *Anal. Chem.* **2021**, *93*, 5377–5382.

18. Li, H.; Du, M.; Mleczko, M. J.; Koh, A. L.; Nishi, Y.; Pop, E.; Bard, A. J.; Zheng, X. Kinetic Study of Hydrogen Evolution Reaction over Strained MoS_2 with Sulfur Vacancies Using Scanning Electrochemical Microscopy. *J. Am. Chem. Soc.* **2016**, *138*, 5123–5129.
19. Jamali, S. S.; Moulton, S. E.; Tallman, D. E.; Weber, J.; Wallace, G. G. Electro-Oxidation and Reduction of H_2 on Platinum Studied by Scanning Electrochemical Microscopy for the Purpose of Local Detection of H_2 Evolution. *Surf. Interface Anal.* **2015**, *47*, 1187–1191.
20. Kund, J.; Romer, J.; Oswald, E.; Gaus, A.-L.; Küllmer, M.; Turchanin, A.; von Delius, M.; Kranz, C. Pd-Modified De-alloyed Au−Ni-Microelectrodes for In Situ and Operando Mapping of Hydrogen Evolution. *ChemElectroChem* **2022**, *9*, e202200071.
21. Koster, D.; Gutkowski, R.; Masa, J.; Schuhmann, W. H_2 Quantification Based on Selective Pre-Concentration and Oxidative Stripping at Pd Modified Microelectrodes. *J. Electroanal. Chem.* **2018**, *812*, 207–212.
22. Wang, Y.; Wipf, D. O. Visualizing Hydrogen Oxidation Reaction Activity of Polycrystalline Platinum by Scanning Electrochemical Microscopy. *J. Electrochem. Soc.* **2020**, *167*, 146502.
23. Zoski, C. G. Scanning Electrochemical Microscopy: Investigation of Hydrogen Oxidation at Polycrystalline Noble Metal Electrodes. *J. Phys. Chem. B* **2003**, *107*, 6401–6405.
24. Zhou, J.; Zu, Y.; Bard, A. J. Scanning Electrochemical Microscopy: Part 39. The Proton/Hydrogen Mediator System and its Application to the Study of the Electrocatalysis of Hydrogen Oxidation. *J. Electroanal. Chem.* **2000**, *491*, 22–29.
25. Djire, A.; Wang, X.; Xiao, C.; Nwamba, O. C.; Mirkin, M. V.; Neale, N. R. Basal Plane Hydrogen Evolution Activity from Mixed Metal Nitride MXenes Measured by Scanning Electrochemical Microscopy. *Adv. Funct. Mater.* **2020**, *30*, 2001136.
26. Sun, T.; Zhang, H.; Wang, X.; Liu, J.; Xiao, C.; Nanayakkara, S. U.; Blackburn, J. L.; Mirkin, M. V.; Miller, E. M. Nanoscale Mapping of Hydrogen Evolution on Metallic and Semiconducting MoS_2 Nanosheets. *Nanoscale Horiz.* 2019, 4, 619–624.
27. Sun, T.; Yu, Y.; Zacher, B. J.; Mirkin, M. V. Scanning Electrochemical Microscopy of Individual Catalytic Nanoparticles. *Angew. Chem. Int. Ed.* **2014**, *53*, 14120–14123.
28. Niu, H.-J.; Yan, Y.; Jiang, S.; Liu, T.; Sun, T.; Zhou, W.; Guo, L.; Li, J. Interfaces Decrease the Alkaline Hydrogen-Evolution Kinetics Energy Barrier on NiCoP/Ti_3C_2Tx MXene. *ACS Nano* **2022**, *16*, 11049–11058.
29. Kim, J.; Renault, C.; Nioradze, N.; Arroyo-Currás, N.; Leonard, K. C.; Bard, A. J. Electrocatalytic Activity of Individual Pt Nanoparticles Studied by Nanoscale Scanning Electrochemical Microscopy. *J. Am. Chem. Soc.* **2016**, *138*, 8560–8568.
30. Bard, A. J. Inner-Sphere Heterogeneous Electrode Reactions. Electrocatalysis and Photocatalysis: The Challenge. *J. Am. Chem. Soc.* **2010**, *132*, 7559–7567.

31. Nioradze, N.; Chen, R.; Kurapati, N.; Khvataeva-Domanov, A.; Mabic, S.; Amemiya, S. Organic Contamination of Highly Oriented Pyrolytic Graphite As Studied by Scanning Electrochemical Microscopy. *Anal. Chem.* **2015**, *87*, 4836–4843.
32. Barman, K.; Wang, X.; Jia, R.; Mirkin, M. V. Mediated Charge Transfer at Nanoelectrodes: A New Approach to Electrochemical Reactivity Mapping and Nanosensing. *J. Am. Chem. Soc.* **2021**, *143*, 8547–8551.
33. Gu, C. Q.; Sun, T.; Wang, Z. Y.; Jiang, S. S.; Wang, Z. H. High Resolution Electrochemical Imaging for Sulfur Vacancies on 2D Molybdenum Disulfide. *Small Methods* **2023,** *7*, 8.
34. Barman, K.; Wang, X.; Jia, R.; Askarova, G.; Hu, G. X.; Mirkin, M. V. Voltage-Driven Molecular Catalysis of Electrochemical Reactions. *J. Am. Chem. Soc.* **2021,** *143*, 17344–17347.
35. Mirkin, M. V.; Wang Y. Theory. In Scanning Electrochemical Microscopy, 3rd ed.; Bard, A. J.; Mirkin, M. V., Eds.; CRC Press: Boca Raton, 2022, pp. 65-103.
36. Shaner, M. R.; Atwater, H. A.; Lewis, N. S.; McFarland, E. W. A Comparative Technoeconomic Analysis of Renewable Hydrogen Production Using Solar Energy. *Energy Environ. Sci.* **2016**, 9, 2354−2371.
37. Shoup, D.; Szabo, A. Influence of Insulation Geometry on the Current at Microdisk Electrodes. *J. Electroanal. Chem.* **1984**, *160*, 27–31.
38. Vivian, J.E.; King, C.J. The Mechanism of Liquid-Phase Resistance to Gas Absorption in a Packed Column. *AIChE J*. **1964**, *10*, 221–227.
39. Butler, I. B.; Schoonen, M. A. A.; Rickard, D. T. Removal of Dissolved Oxygen from Water: A Comparison of Four Common Techniques. *Talanta* **1994**, *41*, 211–215.
40. Craig, V. S. Gas Solubility of Electrolytes. In Encyclopedia of Applied Electrochemistry; Kreysa, G.; Ota, K.I.; Savinell, R. F., Eds.; Springer: New York, 2014, pp. 927-931.
41. Schumpe, A.; Adler, I.; Deckwer, W.-D. Solubility of Oxygen in Electrolyte Solutions. *Biotechnol. Bioeng.* **1978**, *20,* 145-150.
42. Snook, G. A.; Duffy, N. W.; Pandolfo, A. G. Detection of Oxygen Evolution from Nickel Hydroxide Electrodes Using Scanning Electrochemical Microscopy. *J. Electrochem. Soc.* **2008**, *155*, A262.
43. Askarova, G.; Xiao, C.; Barman, K.; Wang, X.; Zhang, L.; Osterloh, F. E.; Mirkin, M. V. Photo-Scanning Electrochemical Microscopy Observation of Overall Water Splitting at a Single Aluminum-Doped Strontium Titanium Oxide Microcrystal. *J. Am. Chem. Soc.* **2023**, *145*, 6526–6534.
44. Askarova, G.; Hesari, M.; Barman, K.; Mirkin, M. V. Visualizing Overall Water Splitting on Single Microcrystals of Phosphorus-Doped $BiVO_4$ by Photo-SECM. *ACS Appl. Mater. Interfaces* **2023**, *15*, 47168–47176.

45. Bard, A. J.; Mirkin, M. V.; Unwin, P. R.; Wipf, D. O. Scanning Electrochemical Microscopy. 12. Theory and Experiment for Finite Heterogeneous Electron Transfer Kinetics and Arbitrary Substrate Size. *J. Phys. Chem.* **1992**, *96*, 1861−1868.
46. Xiong, H.; Guo, J.; Amemiya, S. Probing Heterogeneous Electron Transfer at an Unbiased Conductor by Scanning Electrochemical Microscopy in the Feedback Mode. *Anal. Chem.* **2007**, *79*, 2735−44.
47. Sun, P.; Mirkin, M. V. Kinetics of Electron Transfer Reactions at Nanoelectrodes. *Anal. Chem.* **2006**, *78*, 6526–6534.
48. Nioradze, N.; Chen, R.; Kim, J.; Shen, M.; Santhosh, P.; Amemiya, S. Origins of Nanoscale Damage to Glass-Sealed Platinum Electrodes with Submicrometer and Nanometer Size. *Anal. Chem*. **2013**, *85*, 6198–6202.
49. Wang, X.; Han, L.; Xin, H.; Mirkin, M. V. TEM-Assisted Fabrication of Sub-10 nm Scanning Electrochemical Microscopy Tips. *Anal. Chem.* **2019**, *91*,15355–15359.
50. Barnes, J. T.; Griffith, K. J.; Beeler, J. A.; Gerroll, B. H.; Petro, A. G. C.; Williams, C. G.; Siedle, A. R.; Tait, S. L.; Peters, D. G. Alkyl-Group Grafting onto Glassy Carbon Cathodes by Reduction of Primary Monohaloalkanes: Electrochemistry and X-ray Photoelectron Spectroscopy Studies. *J. Electroanal. Chem.* **2020**, *856*, 113531.
51. Bo, T.; Wang, X.; Jia, R.; Han, L.; Xin, H. L.; Zhang, H.; Miller, E. M.; Mirkin, M. V. Probing Activities of Individual Catalytic Nanoflakes by Tunneling Mode of Scanning Electrochemical Microscopy. *J. Phys. Chem. C* **2021**, *125*, 25525–25532.
52. Cornut, R.; Lefrou, C. A unified new analytical approximation for negative feedback currents with a microdisk SECM tip. *J. Electroanal. Chem*. **2007**, *608*, 59–66.

TOC graphic